

# Learning to Extend Molecular Scaffolds with Structural Motifs

Krzysztof Maziarz<sup>1</sup> Henry Jackson-Flux<sup>1</sup> Pashmina Cameron<sup>1</sup>  
 Finton Sirockin<sup>2</sup> Nadine Schneider<sup>2</sup> Nikolaus Stieff<sup>2</sup> Marc Brockschmidt<sup>1</sup>

## Abstract

Recent advancements in deep learning-based modeling of molecules promise to accelerate *in silico* drug discovery. There is a plethora of generative models available, which build molecules either atom-by-atom and bond-by-bond or fragment-by-fragment. Many drug discovery projects also require a fixed scaffold to be present in the generated molecule, and incorporating that constraint has been recently explored. In this work, we propose a new graph-based model that learns to extend a given partial molecule by flexibly choosing between adding individual atoms and entire fragments. Extending a scaffold is implemented by using it as the initial partial graph, which is possible because our model does not depend on generation history. We show that training using a randomized generation order is necessary for good performance when extending scaffolds, and that the results are further improved by increasing fragment vocabulary size. Our model pushes the state-of-the-art of graph-based molecule generation, while being an order of magnitude faster to train and sample from than existing approaches.

## 1. Introduction

The problem of *in silico drug discovery* requires navigating a vast chemical space in order to find molecules of interest that satisfy various constraints on their properties and structure. This poses challenges well beyond those solvable by brute-force search, leading to the development of more sophisticated approaches. Recently, deep learning models are becoming an increasingly popular choice, because they can *learn* a distribution over drug-like molecules from raw data.

Generative modeling of molecules can be performed by using an auto-encoder model (Kingma & Welling, 2013), created by pairing an encoder with a matching decoder. While classical models rely on a textual SMILES notation to rep-

<sup>1</sup>Microsoft Research, Cambridge, UK <sup>2</sup>Novartis Institutes for BioMedical Research, Novartis Pharma AG, Novartis Campus, 4002 Basel, Switzerland. Correspondence to: Krzysztof Maziarz <krzysztof.maziarz@microsoft.com>.

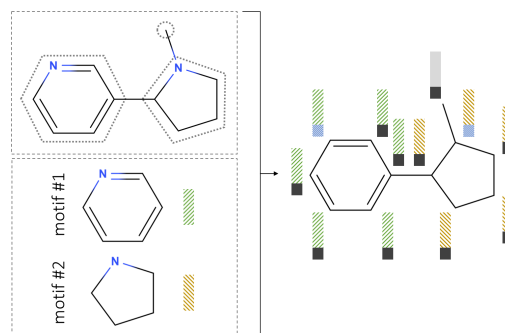


Figure 1. Overview of how an example molecule (top left) is processed, conditioned on the motif vocabulary (bottom left) to make the motif information readily available at the atom level (right). Each atom is associated with a feature vector, which consists of atom-level features (bottom part) and a motif embedding (top part).

resent molecules (Segler et al., 2018; Gómez-Bombarelli et al., 2018; Winter et al., 2019a), many recent approaches are using molecular graphs (Liu et al., 2018; Jin et al., 2018; 2020). The latter direction gave rise to several graph generative models, where the encoder is implemented by a Graph Neural Network (GNN) (Scarselli et al., 2008), and the decoder reconstructs the input graph either sequentially (Liu et al., 2018) or in a one-shot manner (De Cao & Kipf, 2018). Compared to SMILES-based methods, graph-based models that employ a sequential decoder enjoy perfect validity of generated molecules, as they can enforce valence constraints during generation.

However, even if a molecule does not violate valence constraints, it is merely a sign of syntactic validity; the molecule can still be semantically incorrect by containing unstable or unsynthesizable substructures. Intermediate states during atom-by-atom generation may contain atypical chemical fragments, such as alternating bond patterns corresponding to unfinished aromatic rings (Jin et al., 2018). Therefore, some works (Rarey & Dixon, 1998; Jin et al., 2018; 2020) propose data-driven methods to mine common molecular fragments – referred to as *motifs* – which can be used to build molecules fragment-by-fragment instead of atom-by-atom. When motifs are employed, most partial molecules during generation are semantically sensible, since they do not contain half-built structures such as partial rings.

On the other hand, a common additional constraint in drug discovery projects is the inclusion of a predefined subgraph (called a *scaffold*). Generating molecules that contain a given scaffold can be approached by drawing many samples and discarding those that do not contain the scaffold – while simple, this method is not scalable, as the number of samples required may grow exponentially with scaffold size. Instead, recent models can generate molecules that are bound to contain a given scaffold (Lim et al., 2019; Li et al., 2019; Arús-Pous et al., 2020; Langevin et al., 2020).

Extending a generative model to perform scaffold-based generation is often non-trivial. Ideally, one would train the model without explicitly considering scaffolds, and then constrain the decoding procedure to contain the scaffold with certainty. This is possible for models equipped with a sequential graph decoder, which can be initialized with a scaffold as the starting partial graph. For this operation to be feasible, the model must satisfy the following constraints: (a) it should be trained with a broad range of generation orders, so that possible scaffolds naturally occur as prefixes of the generation order, and thus are among the partial graphs encountered during training, and (b) it cannot be fully autoregressive by depending on generation history, for example by passing along recurrent state, as such state is not available if generation is initialized with a scaffold. While one could side-step (b) by running through a teacher-forced order to obtain the recurrent state, the exact way the scaffold is traversed may bias subsequent generation.

However, current state-of-the-art fragment-based models (Jin et al., 2018; 2020) cannot be initialized with a scaffold, as they violate (a) by relying on a deterministic molecule generation order (such as a depth-first search (DFS) ordering). Some models (Jin et al., 2018) also do not satisfy (b), due to using gated recurrent units (GRUs) (Cho et al., 2014) which contain recurrent state.

In this work, we explore the design space of graph-based generative models of molecules that can initialize decoding from a scaffold. In line with recent state-of-the-art approaches (Jin et al., 2018; 2020), we focus on motif-based generation. We make the following contributions:

- We design a new graph generative model that utilizes structural motifs. In contrast to prior work (Jin et al., 2018; 2020), our model can still generate arbitrary structures atom-by-atom, removing the reliance on the motif vocabulary to cover all useful rings.
- Instead of designing a scaffold-specific model or training paradigm, we explicitly consider the aforementioned constraints; we show that satisfying (a) is necessary and sufficient for our family of models to retain good performance even when initialized from an arbitrary scaffold.

- We identify two crucial design decisions that are understudied in the current literature: the choice of the generation order and the size of the motif vocabulary. We then show how varying these two parameters affects various aspects of downstream model performance. Our experiments span both scaffold-constrained and unconstrained molecule generation.

We refer to the family of proposed models as the MoLeR models, since in contrast to HierVAE (Jin et al., 2020) the next decoding step is conditioned on the current partial graph through a single **M**olecule-**L**evel **R**epresentation. The motif information is made available at the atom level, and can inform all message passing steps; we schematically show this in Figure 1 and explain in detail in Section 3.1.

## 2. Background

We represent a molecule using a molecular graph  $\mathcal{G} = (\mathcal{V}, \mathcal{E})$ , where vertices  $\mathcal{V}$  correspond to atoms, and edges  $\mathcal{E}$  to bonds. Additionally, each atom  $v \in \mathcal{V}$  may be associated with an atom feature vector  $a_v$  that encodes chemically relevant features, such as atom type, aromaticity, or presence of rings. Each bond may also be annotated with extra features, although here we follow prior work (Liu et al., 2018; Jin et al., 2018; 2020) and associate bonds only with bond type, which is represented as a categorical feature with three classes (single, double, and triple).

**Graph Neural Networks** Models that act on molecular graphs often propagate information using a Graph Neural Network (GNN) (Li et al., 2015; Kipf & Welling, 2016). The network is initialized with starting node representations  $\{h_v^0 : v \in \mathcal{V}\}$ ; in our case, these representations are set to linear projections of  $a_v$ . Each GNN layer propagates node representations  $\{h_v^t : v \in \mathcal{V}\}$  to compute  $\{h_v^{t+1} : v \in \mathcal{V}\}$  using message passing (Gilmer et al., 2017):

$$h_v^{t+1} = f(h_v^t, a(\{m_l(h_v^t, h_u^t) : (v, l, u) \in \mathcal{E}\}))$$

where  $m_l$  computes the message between two nodes connected by an edge of type  $l$ ,  $a$  aggregates the messages received by a given node, and  $f$  computes the new state based on previous state and aggregated messages. A common choice is to use a linear layer for  $m_l$ , a pointwise sum for  $a$ , and a GRU update for  $f$  (Li et al., 2015), but many other variants were explored (Corso et al., 2020). After  $L$  layers of message passing we obtain final representations  $\{h_v^L : v \in \mathcal{V}\}$ , with  $h_v^L$  summarizing the  $L$ -hop neighborhood of  $v$ . These representations can be pooled to form a graph-level representation by using any permutation-invariant aggregator, such as a weighted sum.

### 3. Our approach

#### 3.1. Data

**Motif vocabulary** Training our model relies on a set of fragments  $\mathcal{M}$  – called the *motif vocabulary* – which we infer directly from data. Note that in contrast to Jin et al. (2018; 2020) we do not assume that  $\mathcal{M}$  covers all useful cycles, and thus setting  $\mathcal{M} = \emptyset$  is valid.

For each training molecule, we decompose it into fragments by breaking some of the bonds. As breaking apart rings is chemically challenging, we only consider *acyclic bonds*, i.e. bonds that do not lie on any cycle. We break all acyclic bonds adjacent to a cycle (i.e. at least one endpoint lies on a cycle), as that separates the molecule into cyclic substructures, such as ring systems, and acyclic substructures connected to them, such as some functional groups. We then aggregate the resulting fragments over the entire training set and define the motif vocabulary  $\mathcal{M}$  by choosing  $n$  most common motifs, where  $n$  is a hyperparameter.

Having selected  $\mathcal{M}$ , we pre-process molecules (both for training and inference) by noting which atoms are covered by motifs belonging to the vocabulary. This is done by applying the same bond breaking procedure as used for motif vocabulary extraction. During generation, each group of atoms that make up a motif is generated in one step, while remaining atoms and bonds are generated one-by-one. This means that MoLeR has the flexibility to generate an arbitrary structure, such as an unusual ring, even if it does not commonly appear in training data.

Finally, note that in contrast to HierVAE (Jin et al., 2020), we do not decompose ring systems into individual rings. This means that motifs found in a molecule are atom-disjoint, while HierVAE allows motifs to intersect on several atoms. As a consequence, we do not need to model a motif-specific attachment point vocabulary, as attaching a motif to a partial graph requires adding only a single bond, and thus there is only one attachment point.

**Atom features** To process molecules with a GNN, we featurize the atoms and compute atom features  $a_v$  (Pocha et al., 2020). We produce  $a_v$  from several chemically relevant features, including those specific to a given atom (its type, charge, mass, valence, and isotope information) and describing local neighborhood (aromaticity and presence of rings of specific sizes). These features can be readily extracted using the RDKit library (Landrum et al., 2006). Additionally, for atoms that are part of a motif, we concatenate  $a_v$  with the motif embedding; for the other atoms, we concatenate with a special embedding vector to signify the lack of a motif. We show this in Figure 1. Motif embeddings are learned end-to-end with the rest of the model, similarly to word embeddings (Mikolov et al., 2013).

---

#### Algorithm 1 Computing a generation order of a molecule

---

```

Input: molecule  $mol$ , motif annotations
 $order : \text{List}[\text{Atom}] = []$ 
 $choices : \text{List}[\text{List}[\text{Atom}]] = []$ 
 $partial : \text{Mol} = \emptyset$ 
while  $partial \neq mol$  do
  if  $partial = \emptyset$  then
     $nextChoices = \text{ValidFirstAtoms}(mol)$ 
  else
     $nextChoices = \text{ValidNextAtoms}(mol, partial)$ 
  end if
  Append  $nextChoices$  to  $choices$ 
  Choose  $nextAtom$  randomly from  $nextChoices$ 
  if  $nextAtom$  is covered by a motif then
     $atomsToAdd = \text{motif covering } nextAtom$ 
  else
     $atomsToAdd = [nextAtom]$ 
  end if
  Add  $atomsToAdd$  to  $order$  and  $partial$ 
end while

```

---

#### 3.2. Generation order

For each training molecule, we decompose it into a sequence of generation steps. We interleave adding an atom or motif to the partial graph, and adding bonds to connect the newly added structure to the rest of the molecule.

A single molecule may be generated in a variety of different orders, ranging between fully deterministic and fully random. We decompose selecting the generation order into two steps: first choosing a starting atom, then for every partial graph (submolecule) choosing the next atom from the *frontier*, i.e. unvisited atoms adjacent to the current partial graph. After each choice, if the currently selected atom is part of a motif, we add the entire motif into the partial graph at once. We formalize this concept as pseudocode in Algorithm 1.

Our formalism permits a variety of orders, in particular, any deterministic order dependent only on the input molecule can be trivially cast as Algorithm 1, by making ValidFirstAtoms and ValidNextAtoms return singletons. This includes orders commonly used in the literature, such as canonical, breadth-first (BFS) and depth-first (DFS) orders. In this work, we evaluate the following orders: *random*, where ValidFirstAtoms returns all atoms and ValidNextAtoms all atoms on the frontier on the current partial graph, which covers all valid generation orders; *canonical*, which is fully deterministic and follows a canonical ordering (Schneider et al., 2015) of the atoms computed using RDKit; and two variants of *BFS*, where we choose the first atom either randomly or as the first atom in canonical order, and then explore the remaining atoms in BFS order, breaking ties between equidistant next nodes randomly.

### 3.3. Model

Our model follows the autoencoder paradigm. Both encoder and decoder are graph-based (hence invariant to the order of atoms) and featurize input data as defined in Section 3.1.

Note that, while our GNNs are not hierarchical, they are motif-aware, as motif annotations are present in atom features. While these annotations are deterministic functions of the input molecule, and thus in principle could be learned by the GNN itself, we found them to be crucial to achieve good performance. For message passing, we use a simple yet expressive GNN-MLP layer, which computes messages for each edge by passing the states of its endpoints through an MLP. Brockschmidt (2020) showed that this simple approach matches or outperforms commonly used GNN layers such as GCN (Kipf & Welling, 2016) or GIN (Xu et al., 2018). However, our model is agnostic to the GNN layer type.

Our encoder  $q_\theta(z|x)$  is implemented by a GNN followed by an aggregation layer, with two heads used to parameterize the mean and the standard deviation of the latent code  $z$ . The decoder  $p_\phi(x|z)$  decomposes the generation of  $x$  in a partially auto-regressive manner. The current state of generation is characterized by a pair  $(g_i, v_i)$ , where  $g_i \subseteq x$  is a partial graph spanning nodes  $\mathcal{V}_i \subseteq \mathcal{V}$ , and  $v_i \in \mathcal{V}_i \cup \{\perp\}$  is either a *focus node* selected in  $g_i$  or a symbol  $\perp$  to signal the lack of focus node. If the state has a focus node  $v_i$ , it means we are currently generating new edges from  $v_i$  to the rest of  $g_i$ . Once the network predicts that no more edges should be added, we move to a state without a focus node, meaning that either a new node should be added, or generation should halt.

Denote the sequence of states that result in  $x$  by  $(\emptyset, \perp) = s_0, s_1, \dots, s_k = (x, \perp)$ , and let  $a_i$  be the action that transforms  $s_i$  into  $s_{i+1}$ . Then the probability of generating  $x$  is decomposed as follows:

$$\log p_\phi(x|z) = \sum_i \log p(a_i|z, s_i) \quad (1)$$

Note that the distribution over the next action  $a_i$  is conditioned only on the latent vector  $z$  and the current partial graph  $g_i$ . Our decoding is therefore not fully auto-regressive, as there is no direct dependence of  $a_i$  on  $a_{<i}$ . We now elaborate on the actions  $a_i$ , and how their prediction is modeled.

Our decoder processes  $(g_i, v_i)$  using a GNN, which results in high-level features  $f_v$  for each atom in  $\mathcal{V}_i$ , and an aggregated feature vector  $f_{mol}$ . Depending on  $v_i$ , the decoder then makes one of three kinds of predictions:

- If  $v_i = \perp$ , the decoder performs *next node prediction*, to choose the next atom or motif to be added to  $g_i$ , with

an extra class to signify that no more nodes should be added. As seen in Algorithm 1, some of the generation orders we consider are randomized, choosing the next node to explore from a list of candidates. Therefore, we model the next node prediction as a classification task with a multi-hot objective, using *nextChoices* to construct the target. In practice, this prediction is implemented with an MLP, taking  $f_{mol}||z$  as input.

- If the next node prediction step chooses to add a motif, we perform an additional *attachment prediction* step, which predicts one of the endpoints of a new bond connecting the motif with  $g_i$ . In contrast to Jin et al. (2020), our motifs are atom-disjoint; therefore, we only need to choose a *single atom* in the newly added motif as an attachment point, which becomes the focus node  $v_i$ . We implement this selection with an MLP, which scores every node  $v$  in the newly added motif<sup>1</sup>, given as input  $f_{mol}||z||f_v$ .
- Finally, if  $v_i \neq \perp$ , we predict new bonds from  $v_i$ . In each step, we either predict that a new bond should be added, or that generation should continue (by setting the focus node back to  $\perp$ ). This is implemented with an MLP to score all potential next bonds from  $v_i$ , and potential bond types, where scoring the  $(v_i, u)$  bond is conditioned on  $f_{mol}||z||f_{v_i}||f_u$ . Similarly to Liu et al. (2018), we employ valence checks to mask out bonds that would lead to chemically invalid molecules. Moreover, if  $v_i$  was selected as an attachment point in a motif, we mask out edges to other atoms in the same motif; for example, if the motif is a ring, we disallow extending it with extra chords.

### 3.4. Training objective

We train our model to optimize a standard VAE loss (Kingma & Welling, 2013) with several modifications, resulting in a linear combination of three terms:  $\mathcal{L}_{rec}(x)$ , which ensures the input molecule  $x$  can be approximately reconstructed from an encoding  $z \sim q_\theta(z|x)$ ;  $\mathcal{L}_{prior}(x)$ , which regularizes the encoder distribution  $q_\theta(z|x)$  to stay close to the prior  $p(z)$  (here a multivariate Gaussian); and  $\mathcal{L}_{prop}(x)$ , which ensures that chemical properties can be accurately predicted from the latent encoding of a molecule. We now elaborate on each of these loss components.

According to Equation 1, the reconstruction term  $\mathcal{L}_{rec}$  should be a sum over all generation steps. However, we instead rewrite this term as an expectation with the step chosen uniformly over the entire generation:

$$\mathcal{L}_{rec}(x) = \mathbb{E}_{z \sim q_\theta(z|x)} \mathbb{E}_{i \sim \mathcal{U}} \log p(a_i|z, s_i) \quad (2)$$

<sup>1</sup>In practice, we first determine motif symmetries using RDKit, and then score one atom per equivalence class.

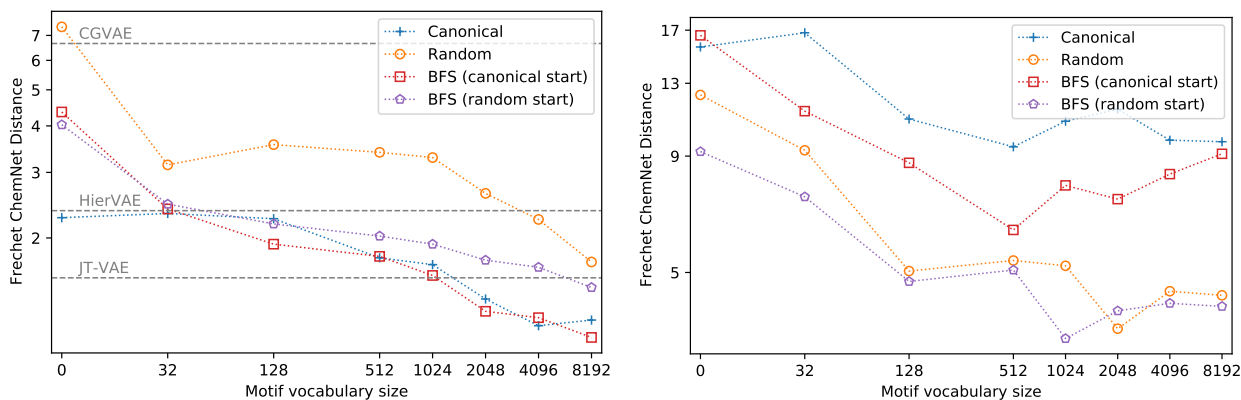


Figure 2. Frechet ChemNet Distance (lower is better) across different generation orders and motif vocabulary sizes. We consider both generation from scratch (left), and generation starting from a pre-defined scaffold (right).

This rewriting makes it explicit that different generation steps for a fixed input molecule do not depend on each other. This enables two improvements: parallel training on all generation steps at once, and subsampling the steps (i.e. using only a subset of steps per input molecule) to get more variety within each batch. These enhancements improve training speed and robustness, and are feasible precisely because our model does not depend on history.

Next, we define  $\mathcal{L}_{prior}(x) = -\mathcal{D}_{KL}(q_{\theta}(z|x)||p(z))$ , and follow Higgins et al. (2016) in adding a  $\beta$  hyperparameter to weigh down that part of the loss; in preliminary experiments, we found that using  $\beta < 1$  makes the training much more stable and improves results significantly.

Finally, following prior works (Gómez-Bombarelli et al., 2018; Winter et al., 2019a; Li et al., 2021), we implement  $\mathcal{L}_{prop}(x)$  using an MLP regressor that predicts molecular weight, synthetic accessibility (SA) score, and octanol-water partition coefficient (logP). All of these properties can be readily computed from the input molecule  $x$  using the RD-Kit library, and hence do not require additional annotations in the training data. Note that due to the inherent stochasticity in the VAE encoding process, obtaining a low value of  $\mathcal{L}_{prop}$  is only possible if the latent space learned by  $q_{\theta}$  is smooth with respect to the predicted properties.

## 4. Experiments

### 4.1. Setup

We use training data from GuacaMol (Brown et al., 2019), which released a curated set of approximately 1.5M drug-like molecules, divided into train, validation and test sets. We train MoLeR on the GuacaMol training set, using the validation set loss as the criteria for early stopping. We construct graph batches so that the total number of nodes per batch does not exceed 25k. After early stopping is

triggered, we use the single best checkpoint selected based on validation loss to evaluate on downstream tasks. For more details on the model architecture, experimental setup, and hyperparameters, see Appendix A.

Moreover, we found that subsampling the training steps and using only half of the steps per molecule tends to speed up convergence and lead to a lower final loss, as it yields more variety within each batch. Therefore, we subsample training steps for all MoLeR experiments unless noted otherwise.

**Baselines** As baselines, we consider three established graph-based generative models: CGVAE (Liu et al., 2018), JT-VAE (Jin et al., 2018), and HierVAE (Jin et al., 2020).

Since the publicly released code of Liu et al. (2018) does not scale to datasets as large as GuacaMol, for the sake of a fair comparison we re-implemented CGVAE following the released code to make it more efficient. For JT-VAE, we used the open-source code, but implemented multithreaded decoding, which made sampling 8x faster. For HierVAE, we used the released code with no changes. Due to the high cost of training JT-VAE and HierVAE, we did not tune their hyperparameters and instead used the default values.

### 4.2. Results

**Training and sampling speed** We measure how efficient our architecture is, both in terms of training and sampling from the prior. In both cases, we measure the number of molecules processed per second. Note that we do *not* subsample training steps for this comparison, so that every model processes all the steps, even though MoLeR can learn from only a subset of them. We compare these results in Table 1. We see that, thanks to a simpler formulation and parallel training on all generation steps, MoLeR is much faster than all baselines for both training and inference.

Table 1. Training and sampling speed for our model and the baselines, all measured on a single Tesla K80 GPU.

MODEL	TRAIN (MOL/SEC)	SAMPLE (MOL/SEC)
CGVAE	57.0	1.4
JT-VAE	3.2	3.4
HIERVAE	17.0	12.3
MoLER	<b>95.2</b>	<b>34.2</b>

**Generation** Similarly to Brown et al. (2019), we use Frechet ChemNet Distance (FCD) (Preuer et al., 2018) to measure how well the molecules sampled from a trained model resemble those in the training data. We consider two scenarios: sampling molecules from the prior, and sampling starting from a scaffold.

For generation from scratch, we decode random latent samples from the VAE prior and compare them to a random sample from the data. We show the results in Figure 2 (left). We see that random order performs poorly, as it has to model a much harder problem of generation under a wide range of different orders, and this does not seem to benefit the downstream sampling task. We get the best results with orders that choose the starting point deterministically. Moreover, all orders improve when the vocabulary size is increased, showing that motif-based generation is widely beneficial.

Finally, note that MoLeR with a large vocabulary size outperforms all baselines, despite being much faster to train and sample from, and having support for scaffold-constrained generation.

Next, we consider scaffold-constrained sampling, where our goal is to check if the model can recover the subspace of the training distribution consisting of molecules that contain a particular scaffold. To that end, we first choose a chemically relevant scaffold  $s$  (PubChem CID 12658820) that commonly appears in GuacaMol training data. We then estimate the posterior distribution on latent codes induced by  $s$  by encoding all training molecules that contain it and then approximating the resulting latents with a Gaussian Mixture Model (GMM) with 50 mixture components. Finally, we draw latent samples from that distribution, decode them starting the generation process from  $s$ , and compare the resulting molecules with molecules from the data that contain  $s$ . By using samples from the GMM-approximated posterior, as opposed to samples from the prior, we ensure that we use latent codes which are *compatible* with the scaffold  $s$ , which we found to dramatically improve the downstream metrics. Intuitively, constraining the decoding with a scaffold projects the resulting molecule onto a manifold defined by the scaffold constraint; using an approximate posterior makes sure that the projected samples lie close to that manifold. In Figure 2 (right) we show the resulting FCD. We find

that the relative performance of different generation orders is largely *reversed*: since the models trained with canonical order can only complete prefixes of that order, they are not well equipped to complete arbitrary scaffolds. On the other hand, models trained with randomized orders are more flexible and handle the task well. As with generation from scratch, using a larger motif vocabulary tends to help, especially if motifs happen to decompose the scaffold into smaller fragments (or even the entire scaffold may appear in the vocabulary). Finally, we note that BFS order using a random starting point gives the best results for this task, while still showing good performance for unconstrained sampling.

Unlike some prior work (De Cao & Kipf, 2018; Brown et al., 2019), we do not compare validity, uniqueness and novelty, as all our models get near-perfect results on all these metrics, making comparison meaningless. Concretely, we obtain 100% validity by design (due to the use of valence checks), uniqueness above 99%, and novelty above 97%.

**Optimization** In this work, we aim to deeply explore scaffold-constrained graph generation, and hence leave exploring molecular optimization to future work. As a proof-of-concept, in Appendix B we show a simple experiment that showcases the benefits of scaffold-constrained optimization.

### 4.3. Qualitative analysis

**Unconstrained and constrained interpolation** To test the smoothness of our latent space and analyze how adding the scaffold constraint impacts decoding, we select a non-trivial scaffold (PubChem CID 7375) that commonly appears in drug-like molecules, and two dissimilar molecules  $m_1$  and  $m_2$  that contain it. Then, we compute a linear interpolation between the latent encodings of  $m_1$  and  $m_2$ , and select those intermediate points at which the corresponding decoded molecule changes. We show the resulting interpolation in Figure 3 (top row). We see that the model correctly identifies a smooth transition from  $m_1$  to  $m_2$ . Most of the differences between  $m_1$  and  $m_2$  stem from the fact that the latter contains two additional rings, and we see that rings are consistently added during the interpolation. For example, in the third step, the molecule grows by one extra ring, but of a type that does not appear in  $m_2$ ; in the next step, this ring transforms into the correct type, and is then present in all subsequent steps (a similar pattern can be observed for the other ring). However, we see that some intermediate molecules do not contain the scaffold: although all of the scaffold’s building blocks are present, the interpolation goes through a region in which the model decides to move the NH group to a different location, thus breaking the integrity of the scaffold. This shows that while latent space distance strongly correlates with structural similarity, relying on latent space smoothness alone cannot guarantee the presence

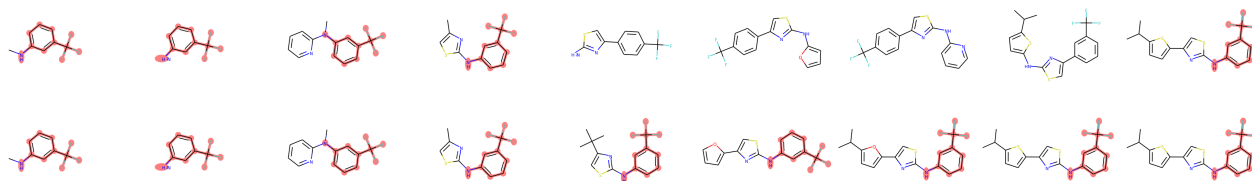


Figure 3. Interpolation between latent encodings of two molecules, both with unconstrained decoding (top) and constrained with scaffold (bottom). The desired scaffold is highlighted in each molecule that contains it.

of a scaffold, which necessitates scaffold-based generation.

In contrast, in Figure 3 (bottom row), we show the same sequence of latent codes, but decoded with a scaffold constraint. We see that the constraint keeps the NH group locked in place, so that all intermediate molecules contain the scaffold. The molecule decoded under a scaffold constraint is typically very similar to the one decoded without, showing that constrained decoding preserves chemical features that are not related to the presence of the scaffold. However, when trying to include the scaffold, our model does not have to resort to a simple rearrangement of existing building blocks: for example, in the 7th step, adding a constraint also modifies one of the ring types, which results in a smoother interpolation in comparison to the unconstrained case. Finally, while the interpolation points were chosen to remove duplicates from the unconstrained path, we observe that the last two latent points both get mapped to  $m_2$  when the scaffold constraint is introduced. This is because the last step of the unconstrained interpolation merely rearranges the motifs, moving back the NH group to its initial location, and restoring the scaffold. This modification is not needed if the scaffold is already present, and therefore our model chooses to project both latent codes to the same point on the scaffold-constrained manifold.

**Latent space neighborhood** To analyze the structure of our scaffold-constrained latent space, we select another chemically relevant scaffold (PubChem CID 57732551), and perform scaffold-constrained decoding of a group of neighboring latent points. To select a latent space neighborhood, we take an arbitrary molecule  $m$  that contains the selected scaffold, encode it, and then decode a  $5 \times 5$  grid of neighboring latent codes centered at the encoding of  $m$ . To produce the grid, we choose two random orthogonal directions in the latent space, and then use binary search to select the smallest step size which results in all 25 latent points decoding to distinct molecules. We show the resulting latent neighborhood in Figure 4, where the scaffold is highlighted in each molecule. We see that the model is able to produce reasonable variations of  $m$ , while maintaining local smoothness, as most adjacent pairs of molecules are very

similar. We also find nearby samples that use the same set of motifs, but differ in their alignment; a similar observation was made by Jin et al. (2018). Moreover, we notice that the left-to-right direction is correlated with size, showing that the latent space respects basic chemical properties. If the same 25 latent codes are decoded without the scaffold constraint, only 9 of them end up containing the scaffold, while the other 16 contain similar but different substructures.

**Motif embedding visualisation** To better understand how MoLeR uses motifs, we extract learned motif embeddings from a trained model, in order to analyze if their distance correlates with chemical similarity.

We start with the embedding layer in the *encoder*, which is used to construct atom features. Interestingly, we find that these embeddings do not cluster in any way, and even very similar motifs are assigned distant embeddings. We hypothesize this is due to the use of a simple classification loss function used for reconstruction, which asks to recover the exact motif type, and does not give a smaller penalty for predicting an incorrect but similar motif. Therefore, for two motifs that are similar on the atom level, it may be beneficial to place their embeddings further apart, since otherwise it would be hard for the GNN to differentiate them at all. We hope this observation can inspire future work to scale to very large motif vocabularies, but use domain knowledge to craft a soft reconstruction loss that respects motif similarity.

Now, we turn to a different set of motif embeddings, which we extract from the last layer of the next node prediction MLP in the *decoder*. This results in one weight vector per every output class (i.e. atom and motif types); in contrast to the encoder-side embeddings, the role of these weight vectors is *prediction* rather than *encoding*. We find that pairs of motif embeddings that have high cosine similarity indeed correspond to very similar motifs, which often differ in very subtle details of the molecular graph. We show some of the closest pairs in Figure 5.

Finally, note that the motif embeddings discussed here (both encoder side and decoder side) were trained end-to-end with the rest of the model, and did not have direct access to graph

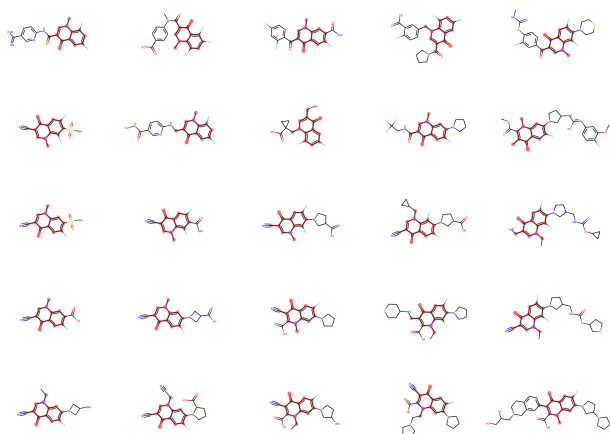


Figure 4. Latent space neighborhood of a fixed molecule containing a chemically relevant scaffold. Each latent code is decoded under a scaffold constraint, so that the desired scaffold (highlighted in red) is present in each molecule.

structure or chemical features of motifs. Therefore, there is no bias that would make embeddings of similar motifs close, and this can only arise as a consequence of training.

## 5. Related work

Our work naturally relates to the rich family of *in silico* drug discovery methods. However, it is most related to works that perform iterative generation of molecular graphs, works that employ fragments or motifs, and works that explicitly consider scaffolds.

**Iterative generation of molecular graphs** Many graph-based models for molecule generation employ some form of iterative decoding, however, usually a single arbitrary ordering is chosen. Liu et al. (2018) first generate all atoms in a one-shot manner, and then generate bonds in BFS order. Jin et al. (2018; 2020) generate a coarsened tree-structured form of the molecular graph in a deterministic DFS order. Finally, You et al. (2018) simply use random order. Mercado et al. (2020) try both random and canonical generation orders, and find the latter produces better samples, which is consistent with our unconstrained generation results.

**Motif extraction** Several other works make use of motif extraction approaches related to the one described in Section 3.1. Jin et al. (2020) propose a very similar strategy, but additionally do not break *leaf bonds*, i.e. bonds incident to an atom of degree 1, which we found produces many motifs that are variations of the same underlying structure (e.g. ring) with different combinations of leaf atoms; for

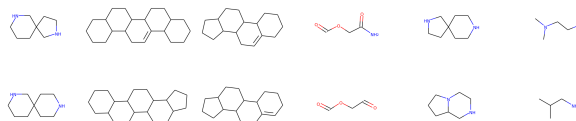


Figure 5. Six pairs of similar motifs (one per column), as extracted from weights of a trained MoLeR model.

simplicity, we chose to omit that rule in our extraction strategy. More complex molecular fragmentation approaches also exist (Degen et al., 2008), and we plan to explore them in future work.

**Motif-based generation** Our work is closely related to the work of Jin et al. (2018; 2020), which also uses motifs to generate molecular graphs. However, these works cannot be easily extended to scaffold-based generation, and cannot generate molecules which use building blocks not covered by the motif vocabulary. While HierVAE (Jin et al., 2020) does include individual atoms and bonds in the vocabulary, their motifs are still assembled in a tree-like manner, meaning that their model cannot generate an arbitrary cyclic structure if not present in the vocabulary.

**Scaffold-conditioned generation** Several prior works can construct molecules under a hard scaffold constraint. Lim et al. (2019) proposes a graph-based model that uses persistent state; scaffold-based generation is possible because the model is explicitly trained on (scaffold, molecule) pairs. This is less sample efficient than MoLeR, which treats *every* intermediate partial graph as if it were a scaffold to be completed. Li et al. (2018) use a soft constraint, where the scaffold is part of the input, but is not guaranteed to be present in the generated molecule. Finally, Arús-Pous et al. (2020); Langevin et al. (2020) rely on SMILES-based models, which need to be explicitly adapted to scaffolds, and cannot guarantee validity of generated molecules.

## 6. Conclusion

In this work, we presented a novel graph-based model for molecular generation. As our model does not depend on history, it can complete arbitrary scaffolds, while still outperforming state-of-the-art graph-based generative models in unconstrained generation. Our quantitative and qualitative results show that our model retains desirable properties of generative models - such as smooth interpolation - while respecting the scaffold constraint. In future work, we plan to explore scaffold-constrained molecular optimization; we believe the sampling efficiency of our model will allow it to tackle real-world optimization problems.

## 7. Acknowledgments

We would like to thank Michal Pikusa and William Jose Godinez Navarro for training the JT-VAE baseline, and Marwin Segler for feedback on an early draft of this work. Moreover, we want to acknowledge the larger team (Hubert Misztela, Jessica Lanini, Megan Stanley, Nikolas Fechner, Richard Lewis and Qurrat Ul Ain) for engaging in helpful discussions.

## References

- Abadi, M., Barham, P., Chen, J., Chen, Z., Davis, A., Dean, J., Devin, M., Ghemawat, S., Irving, G., Isard, M., et al. Tensorflow: A system for large-scale machine learning. In *12th {USENIX} symposium on operating systems design and implementation ({OSDI} 16)*, pp. 265–283, 2016.
- Arús-Pous, J., Patronov, A., Bjerrum, E. J., Tyrchan, C., Reymond, J.-L., Chen, H., and Engkvist, O. Smiles-based deep generative scaffold decorator for de-novo drug design. *Journal of cheminformatics*, 12:1–18, 2020.
- Ba, J. L., Kiros, J. R., and Hinton, G. E. Layer normalization. *arXiv preprint arXiv:1607.06450*, 2016.
- Brockschmidt, M. GNN-film: Graph neural networks with feature-wise linear modulation. In *International Conference on Machine Learning*, pp. 1144–1152. PMLR, 2020.
- Brown, N., Fiscato, M., Segler, M. H., and Vaucher, A. C. Guacamol: benchmarking models for de novo molecular design. *Journal of chemical information and modeling*, 59(3):1096–1108, 2019.
- Cho, K., Van Merriënboer, B., Gulcehre, C., Bahdanau, D., Bougares, F., Schwenk, H., and Bengio, Y. Learning phrase representations using rnn encoder-decoder for statistical machine translation. *arXiv preprint arXiv:1406.1078*, 2014.
- Corso, G., Cavalleri, L., Beaini, D., Liò, P., and Veličković, P. Principal neighbourhood aggregation for graph nets. *arXiv preprint arXiv:2004.05718*, 2020.
- De Cao, N. and Kipf, T. Molgan: An implicit generative model for small molecular graphs. *arXiv preprint arXiv:1805.11973*, 2018.
- Degen, J., Wegscheid-Gerlach, C., Zaliani, A., and Rarey, M. On the art of compiling and using ‘drug-like’ chemical fragment spaces. *ChemMedChem: Chemistry Enabling Drug Discovery*, 3(10):1503–1507, 2008.
- Gilmer, J., Schoenholz, S. S., Riley, P. F., Vinyals, O., and Dahl, G. E. Neural message passing for quantum chemistry. *arXiv preprint arXiv:1704.01212*, 2017.
- Gómez-Bombarelli, R., Wei, J. N., Duvenaud, D., Hernández-Lobato, J. M., Sánchez-Lengeling, B., Sheberla, D., Aguilera-Iparraguirre, J., Hirzel, T. D., Adams, R. P., and Aspuru-Guzik, A. Automatic chemical design using a data-driven continuous representation of molecules. *ACS central science*, 4(2):268–276, 2018.
- Higgins, I., Matthey, L., Pal, A., Burgess, C., Glorot, X., Botvinick, M., Mohamed, S., and Lerchner, A. beta-vaes: Learning basic visual concepts with a constrained variational framework. 2016.
- Jin, W., Barzilay, R., and Jaakkola, T. Junction tree variational autoencoder for molecular graph generation. *arXiv preprint arXiv:1802.04364*, 2018.
- Jin, W., Barzilay, R., and Jaakkola, T. Hierarchical generation of molecular graphs using structural motifs. *arXiv preprint arXiv:2002.03230*, 2020.
- Kingma, D. P. and Ba, J. Adam: A method for stochastic optimization. *arXiv preprint arXiv:1412.6980*, 2014.
- Kingma, D. P. and Welling, M. Auto-encoding variational bayes. *arXiv preprint arXiv:1312.6114*, 2013.
- Kipf, T. N. and Welling, M. Semi-supervised classification with graph convolutional networks. *arXiv preprint arXiv:1609.02907*, 2016.
- Landrum, G. et al. Rdkit: Open-source cheminformatics. 2006. URL <http://www.rdkit.org>.
- Langevin, M., Minoux, H., Levesque, M., and Bianciotto, M. Scaffold-constrained molecular generation. *Journal of Chemical Information and Modeling*, 2020.
- Li, Y., Tarlow, D., Brockschmidt, M., and Zemel, R. Gated graph sequence neural networks. *arXiv preprint arXiv:1511.05493*, 2015.
- Li, Y., Zhang, L., and Liu, Z. Multi-objective de novo drug design with conditional graph generative model. *Journal of cheminformatics*, 10(1):1–24, 2018.
- Li, Y., Hu, J., Wang, Y., Zhou, J., Zhang, L., and Liu, Z. Deepscaffold: A comprehensive tool for scaffold-based de novo drug discovery using deep learning. *Journal of chemical information and modeling*, 60(1):77–91, 2019.
- Li, Y., Ooi, H. K., and Tchagang, A. Deep evolutionary learning for molecular design, 2021. URL [https://openreview.net/forum?id=Fo6S5-3Dx\\_](https://openreview.net/forum?id=Fo6S5-3Dx_).
- Lim, J., Hwang, S.-Y., Kim, S., Moon, S., and Kim, W. Y. Scaffold-based molecular design using graph generative model. *arXiv preprint arXiv:1905.13639*, 2019.

- Liu, Q., Allamanis, M., Brockschmidt, M., and Gaunt, A. Constrained graph variational autoencoders for molecule design. *Advances in neural information processing systems*, 31:7795–7804, 2018.
- Maas, A. L., Hannun, A. Y., and Ng, A. Y. Rectifier nonlinearities improve neural network acoustic models. In *Proc. icml*, volume 30, pp. 3. Citeseer, 2013.
- Mercado, R., Rastemo, T., Lindelöf, E., Klambauer, G., Engkvist, O., Chen, H., and Bjerrum, E. J. Graph networks for molecular design. *Machine Learning: Science and Technology*, 2020.
- Mikolov, T., Chen, K., Corrado, G., and Dean, J. Efficient estimation of word representations in vector space. *arXiv preprint arXiv:1301.3781*, 2013.
- Paszke, A., Gross, S., Massa, F., Lerer, A., Bradbury, J., Chanan, G., Killeen, T., Lin, Z., Gimelshein, N., Antiga, L., Desmaison, A., Kopf, A., Yang, E., DeVito, Z., Raison, M., Tejani, A., Chilamkurthy, S., Steiner, B., Fang, L., Bai, J., and Chintala, S. Pytorch: An imperative style, high-performance deep learning library. In Wallach, H., Larochelle, H., Beygelzimer, A., d'Alché-Buc, F., Fox, E., and Garnett, R. (eds.), *Advances in Neural Information Processing Systems 32*, pp. 8024–8035. Curran Associates, Inc., 2019.
- Pocha, A., Danel, T., and Maziarka, Ł. Comparison of atom representations in graph neural networks for molecular property prediction. *arXiv preprint arXiv:2012.04444*, 2020.
- Preuer, K., Renz, P., Unterthiner, T., Hochreiter, S., and Klambauer, G. Frechet chemnet distance: a metric for generative models for molecules in drug discovery. *Journal of chemical information and modeling*, 58(9):1736–1741, 2018.
- PubChem. Pubchem database. February, 2021. URL <https://pubchem.ncbi.nlm.nih.gov/>.
- PubChem CID 12658820. Pubchem compound summary for cid 12658820 1,4-Dihydroquinoline. January, 2021. URL [https://pubchem.ncbi.nlm.nih.gov/compound/1\\_4-Dihydroquinoline](https://pubchem.ncbi.nlm.nih.gov/compound/1_4-Dihydroquinoline).
- PubChem CID 2244. Pubchem compound summary for cid 2244, aspirin. February, 2021. URL <https://pubchem.ncbi.nlm.nih.gov/compound/Aspirin>.
- PubChem CID 2519. Pubchem compound summary for cid 2519, caffeine. February, 2021. URL <https://pubchem.ncbi.nlm.nih.gov/compound/Caffeine>.
- PubChem CID 57732551. Pubchem compound summary for cid 57732551 1,3-Dimethylquinolin-4(1H)-one. January, 2021. URL [https://pubchem.ncbi.nlm.nih.gov/compound/1\\_3-Dimethylquinolin-4\\_1H-one](https://pubchem.ncbi.nlm.nih.gov/compound/1_3-Dimethylquinolin-4_1H-one).
- PubChem CID 7375. Pubchem compound summary for cid 7375, 3-(trifluoromethyl)aniline. January, 2021. URL <https://pubchem.ncbi.nlm.nih.gov/compound/3-Trifluoromethyl-aniline>.
- Rarey, M. and Dixon, J. S. Feature trees: a new molecular similarity measure based on tree matching. *Journal of computer-aided molecular design*, 12(5):471–490, 1998.
- Scarselli, F., Gori, M., Tsoi, A. C., Hagenbuchner, M., and Monfardini, G. The graph neural network model. *IEEE Transactions on Neural Networks*, 20(1):61–80, 2008.
- Schneider, N., Sayle, R. A., and Landrum, G. A. Get your atoms in order - an open-source implementation of a novel and robust molecular canonicalization algorithm. *Journal of chemical information and modeling*, 55(10):2111–2120, 2015.
- Segler, M. H., Kogej, T., Tyrchan, C., and Waller, M. P. Generating focused molecule libraries for drug discovery with recurrent neural networks. *ACS central science*, 4(1):120–131, 2018.
- Winter, R., Montanari, F., Noé, F., and Clevert, D.-A. Learning continuous and data-driven molecular descriptors by translating equivalent chemical representations. *Chemical science*, 10(6):1692–1701, 2019a.
- Winter, R., Montanari, F., Steffen, A., Briem, H., Noé, F., and Clevert, D.-A. Efficient multi-objective molecular optimization in a continuous latent space. *Chem. Sci.*, 10:8016–8024, 2019b. doi: 10.1039/C9SC01928F. URL <http://dx.doi.org/10.1039/C9SC01928F>.
- Xu, K., Hu, W., Leskovec, J., and Jegelka, S. How powerful are graph neural networks? *arXiv preprint arXiv:1810.00826*, 2018.
- You, J., Liu, B., Ying, R., Pande, V., and Leskovec, J. Graph convolutional policy network for goal-directed molecular graph generation. *arXiv preprint arXiv:1806.02473*, 2018.

## A. Experimental details

### A.1. Architecture

The backbone of our architecture consists of two GNNs: one used to encode the input molecule, and the other used to encode the current partial graph. Both GNNs have the same architecture, but are otherwise completely separate i.e. they do not share any parameters.

To implement our GNNs, we employ the GNN-MLP layer (Brockschmidt, 2020). We use 12 layers with separate parameters, Leaky ReLU non-linearities (Maas et al., 2013), and LayerNorm (Ba et al., 2016) after every GNN layer. After featurizing the atoms, we concatenate the atom features with a motif embedding of size 64, and then linearly project the result back into 64 dimensions, which we maintain as the hidden dimension throughout all GNN layers. Moreover, to improve the flow of gradients in the encoder GNN, we concatenate both initial and intermediate node representations across all layers, obtaining a final node-level feature vector of size  $64 \cdot 13 = 832$ . Intuitively, this concatenation serves as a skip connection that shortens the path from the input graph to the latent encoding  $z$ .

To pool node-level representations into a graph-level representation, we use an expressive multi-headed aggregation scheme. Each aggregation head consists of two MLPs, that for each node compute a scalar score and a transformed version of the node representation:

$$H_i = \{(s_i(f_v), t_i(f_v)) : v \in \mathcal{V}\} \quad (3)$$

We then normalize all scores across the graph, and use them to construct a weighted sum of the transformed representations. To normalize the scores, we consider either passing them through a softmax (which results in a head that implements a weighted mean) or a sigmoid (weighted sum). We use 32 heads for the encoder GNN, and 16 heads for the partial graphs GNN. In both cases, half of the heads use a softmax normalization, while the other half uses sigmoid.

Our node aggregation layer allows to construct a powerful graph-level representation; its dimensionality can be adjusted by varying the number of heads and the output dimension of the transformations  $t_i$ . For input graphs we use a 512-dimensional graph-level representation (which is then transformed to produce the mean and standard deviation of a 512-dimensional latent code  $z$ ), and for partial graphs we use 256 dimensions.

We train our model with the Adam optimizer (Kingma & Ba, 2014). We found that adding an initial warm-up phase for the  $\beta$  coefficient (i.e. increasing it from 0 up to a target value over the course of training) helps to stabilize the model. However, our warm-up phase is relatively short: we reach

the target  $\beta$  in 5000 training steps, whereas full convergence requires around 200 000 steps. This is in contrast to Jin et al. (2018), which varies  $\beta$  uniformly over the entire training. A short warm-up phase is beneficial, as it allows to perform early stopping based on reaching a plateau in validation loss; this cannot be done while  $\beta$  is being varied, as there is no clear notion of improvement if the training objective is changing.

### A.2. Hyperparameter tuning

Due to a very large design space of GNNs, we performed only limited hyperparameter tuning during preliminary experiments. In our experience, improving the modeling (e.g. changing the motif vocabulary or generation order) tends to have a larger impact than tuning low-level GNN architectural choices. For hyperparameters describing the expressiveness of the model, such as the number of layers or hidden representation size, we set them to reasonably high values, which is feasible as our model is very efficient to train. We did not make an attempt to reduce model size; it is likely that a smaller model would give equivalent downstream performance.

One parameter that we found to be tricky to tune is the  $\beta$  coefficient that weighs the  $\mathcal{L}_{prior}$  term of the VAE loss. An additional complication stems from the fact that we compute  $\mathcal{L}_{rec}$  as an average over the generation steps, instead of a sum. While we made this design choice to make the loss scaling robust to training steps subsampling (i.e.  $\beta$  does not have to be adjusted if we use only a subset of steps at training time), it led to decreased robustness when *the difficulty of an average step* varies between experiments. Concretely, when a larger motif vocabulary is used, generating a molecule entails fewer steps, but those steps are harder on average, since the underlying classification tasks need to distinguish between more classes. In preliminary experiments, we noticed the optimal value of  $\beta$  increases with vocabulary size, very closely following a logarithmic trend: doubling the motif vocabulary size translated to the optimum  $\beta$  increasing by 0.005. For the smallest vocabulary sizes (up to 32) we used  $\beta = 0.01$ , and then followed the logarithmic trend described here. Note that, due to the differences in the loss definitions, our value of  $\beta$  is not directly comparable to other  $\beta$ -VAE works.

### A.3. Software and hardware

We performed all experiments on a single GPU. For all measurements in Table 1, we used a machine with a single Tesla K80 GPU.

All of our own implementations (MoLeR, CGVAE) are based on TensorFlow 2 (Abadi et al., 2016), while the models of Jin et al. (2018; 2020) (JT-VAE, HierVAE) use PyTorch (Paszke et al., 2019).

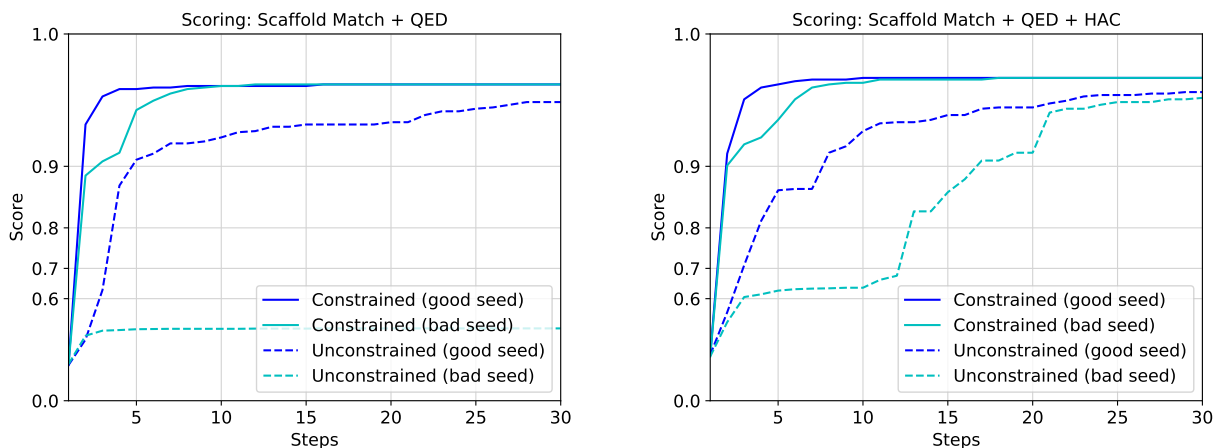


Figure 6. Optimization with/without scaffold constraint (left: optimizing Scaffold Match + QED, right: optimizing Scaffold Match + QED + HAC). Each plot has four curves corresponding to unconstrained and constrained generation for a good and bad seed molecule. In each case, we plot the mean score of the top-10 optimized molecules (higher is better, y-axis is log scale).

## B. Optimization proof-of-concept

We now present a set of results for molecular optimization, as proof-of-concept, to assess how constrained generation compares with unconstrained generation. To perform optimization in the latent space, we use the Molecular Swarm Optimization (MSO) algorithm from Winter et al. (2019b).

We select a chemically relevant scaffold (PubChem CID 57732551), and aim to generate molecules that simultaneously contain the scaffold and have desirable properties. To that end, we use a scoring function that combines three different objectives: Scaffold Match (1 if the molecule contains the scaffold, 0 otherwise), QED (Quantitative Estimate of Drug likeness), and HAC (Heavy Atom Count). To get all objectives into the  $[0, 1]$  range, we map HAC through a piecewise linear function, so that molecules having between 25 and 30 heavy atoms obtain a perfect score of 1, while both below 25 and above 30 the score smoothly decreases to 0.

All of our optimization experiments use a subset of the three loss components described above, which are combined through a simple average. Since all components are in the  $[0, 1]$  range, so is the final combined score.

In Figure 6, we compare optimization runs for constrained and unconstrained generation, starting the search from either of the following seed molecules: Caffeine (PubChem CID 2519) or Aspirin (PubChem CID 2244), which we use as illustrative good and bad seed molecules. The good seed molecule contains a subgraph very similar to the scaffold and consisting of the same atom types, whereas the bad seed molecule does not contain Nitrogen. As the scaffold contains Nitrogen, optimization must learn to add it, in

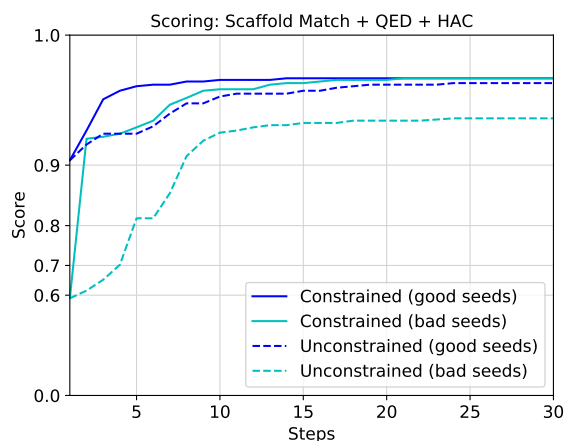


Figure 7. Optimization with/without scaffold constraint for the case when a list of seed molecules is used (optimizing Scaffold Match + QED + HAC). The four curves correspond to unconstrained and constrained generation when starting from a list of 10 good seeds or 10 bad seeds. In each case, we plot the mean score of the top-10 optimized molecules (higher is better, y-axis is log scale).

addition to varying part of the seed molecule to satisfy the scaffold constraint. We see that constraining with scaffold helps irrespective of the choice of the seed molecule, and that starting with a good seed helps for both constrained and unconstrained cases. Further, as constrained generation only returns molecules that satisfy the scaffold constraint, there is less wasted compute in optimizing molecules that obtain low scores due to not containing the scaffold.

Next, we present the results of molecular optimization, in the case where we start with a batch of seed molecules. In Figure 7, we compare optimization runs for constrained and unconstrained generation, starting with two different batches of seed molecules. We use the same scaffold as before, but for this experiment use either 10 good seed molecules or 10 bad seed molecules. We sample each list from a list of all drug-like molecules<sup>2</sup> from PubChem (PubChem), but for the good seeds we first pre-filtered the molecules to only keep those that contain the scaffold. Note that, for each of the four experiments, all seed molecules are utilized within a single optimization run, as MSO can be initialized with a group of starting points, essentially exploring several regions of chemical space simultaneously. Again, we see that constrained generation helps optimize molecules in many fewer steps.

Finally, note that our experiments show that we need fewer *samples* to obtain good results, while in practice, one may be more interested in the *total time* needed. For that comparison, the results for constrained generation are even better, as it generates samples two times faster than unconstrained generation due to part of the molecule being pre-built. Moreover, this speedup grows with scaffold size, and would be even larger if most of the molecule of interest is fixed inside of the scaffold.

---

<sup>2</sup>We use some basic filtering to ensure that the molecules have properties in the usual ranges as expected for drug-like molecules.